Poster2-88

AN OBSERVATIONAL STUDY OF JUMPING CIRRUS WITH GROUND-BASED VISIBLE CAMERAS AND X-BAND RADAR

Takafumi Seguchi [1], Suginori Iwasaki [1]*, Masashi Kamogawa [2], Tomoki Ushiyama [3], Hajime Okamoto [4]

1 Department of Earth and Ocean Sciences, National Defense Academy of Japan, Yokosuka. Kanagawa
2 Global Center for Asian and Regional Research, University of Shizuoka, Shizuoka, Shizuoka
3 International Centre for Water Hazard and Risk Management, Public Works Research Institute, Tsukuba, Ibaraki
4 Research Institute for Applied Mechanics, Kyushu University, Kasuga, Fukuoka

1. INTRODUCTION

Jumping cirrus (JC) is a type of cirrus cloud which literally jumps up from the top of anvil cloud of deep convective storms after the overshooting top (OT) sinks (see Fig. 1 of Seguchi et al., 2019, movies are also available in the paper). The overshooting cloud top usually has colder air than the environment in the lower stratosphere (LS). Thus, it is thought that OTs sink shortly afterward and do not hydrate the LS. On the other hand, some cloud top photography shows that JC appears to partly evaporate above the anvil after drifting away for a while (e.g. Fujita 1974, 1982, and Wang et al. 2009). It may be a visual evidence that JC can transport water vapor atop the anvil directly and/or through a sublimation of ice cloud particles. Some research using satellite observations suggests that the LS above thunderstorms was moist (e.g., Setvák et al., 2008). Recently, the relation between the LS moisture and JC is discussed as JC is likely to contribute to the total amount of stratospheric water vapor and impact the global climate system (Wang et al., 2011).

According to the numerical model studies, it is estimated that JC is generated through the diabatic process, that is, internal gravity wave breaking (IGWB) due to the strong updraft and vertical wind shear above the anvil (e.g., Homeyer et al., 2017, and Wang et al., 2011). However, our knowledge of the physical characteristics of real JC is not sufficient to confirm the mechanism of JC. This is partly because there have been few past observations of JC. Space-borne imagers cannot identify JC since they do not have vertical information and adequate sensitivity for the thin optical thickness of JC. Only a small number of cases, where JC was observed by ground-based cameras, aircraft, space-borne cloud radar and lidar, have been reported at several places worldwide (e.g., Setvák et al., 2013, and Wang et al., 2009), but there were no quantitative studies such as calculations of the height, speed, and duration of the JC. Seguchi et al. (2019) perform the ground-based observations with visible cameras during the summer in Japan and give first-ever analyses of the characteristics of JC based on the ground observation. They suggest that JC can occur even from relatively weak convections like single cell storms, compared with the strong supercell cases in the US, but how the environmental conditions influence the parameters of JC are still not known.

To understand furthermore about JC, the time series of its development, and its relation to the precipitation, this study focuses on the observational analyses for multiple cases of JC, simultaneously using ground-based visible cameras, weather radars, and satellites.

* *Corresponding author address:* Iwasaki Suginori, Dept. of Earth and Ocean Sciences, National Defense Academy, 1-10-20, Hashirimizu, Yokosuka, Kanagawa 239-8686, Japan, e-mail: iwasaki@nda.ac.jp

2. DATA

2.1 *Case Detection of Jumping Cirrus*

The ground-based visible cameras were used to detect the JC cases as described in Seguchi et al. (2019). The method has an advantage that they can record the consecutive change of horizontal and vertical development of cloud with relatively small cost and very high temporal resolution (more than 1 pictures per second). Also, stereo analyses from cameras at different two places can be applicable.

In addition to the 14 cases of JC in 2016 mentioned in Seguchi et al. (2019), we newly found 3 and 11 cases in 2017 and 2018, respectively, by 9 cameras at the summit of Mt. Fuji and the National Defense Academy (NDA, Yokosuka, Japan). Fig. 1 shows the observed area around the Kanto plains with the observation places and where the JC occurred plotted.

Fig. 2 is an example of observed JC by the camera. The grid lines denote the azimuth and elevation angles which are drawn based on the position of stars that cameras took at night. Then, we can determine the direction of an arbitrary object in the photograph. The angular resolution of the camera is 7.5×10^{-3} ° per pixel which corresponds to 10 m at 100 km distant places.

2.2 *Himawari-8*

Using the photographs and the data from the visible band 3 and the infrared band 13 of the Advanced Himawari Imager (AHI) of the geostationary meteorological satellite Himawari-8, the scale of JC such as height, width, velocity, and duration were examined. The AHI has a horizontal resolution of 0.5 km in visible bands and 2 km in infrared bands at

nadir. It scans the whole Japan region every 2.5 minutes.

Fig. 3 illustrates the brightness temperature (BT) of band 13, whose central wavelength is 10.4 μm, around the Kanto when it is 65 seconds after the photograph (Fig. 2). By using the infrared images and azimuth angle of clouds in photos, we can calculate the distances between the observation places and the clouds. It should be noted that we could not see the JC itself due to its small optical thickness in the AHI images. Thus, we alternatively considered the coldest BT point as where JC occurred. By using those distance and angles defined by the photographs, we can calculate spatial scales of the JC.

For the detection of water vapor in the LS, we calculated the brightness temperature difference (BTD) value (Fig. 4) by subtracting the BT of the infrared band 13 from that of the water vapor absorption band 8 of the AHI whose central wavelength is 6.2 μm. If the amount of water vapor in the LS is enough, the BTD value is positive. This is because the air temperature in the LS is warmer than the one at the anvil top layer; hence, the BT of the water vapor absorption band is higher than that of the cloud top.

2.3 *Radiosonde*

The environmental atmospheric conditions when JC occurred were investigated from the radiosonde launched at Tateno (36.06 °N, 140.13 °E). We estimated the altitude of tropopause and the environmental wind shear for the layer between JC and anvil top. The convective available potential energy (CAPE) were also examined as an indicator of updraft strength. Fig. 5 shows an example of the sounding results of the closest time to the photograph (Fig. 2).

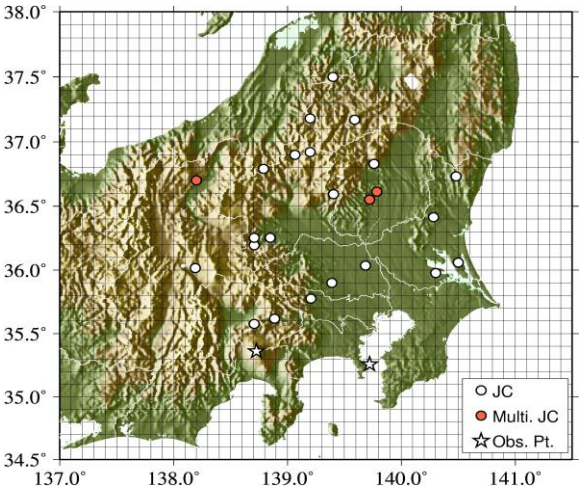

Fig. 1 Observation area and observed JC during the summer of 2016-18. The cameras were set at the summit of Mt. Fuji (35.3 °N, 138.7 °E, 3,776 m above sea level) and at NDA (35.2 °N, 139.7 °E, 100 m above sea level) denoted as star symbols. The coldest BT points of deep convective storms which generated the JC are plotted as circles. The three red circles denote where the multiple JC occurred during the same convective storm.

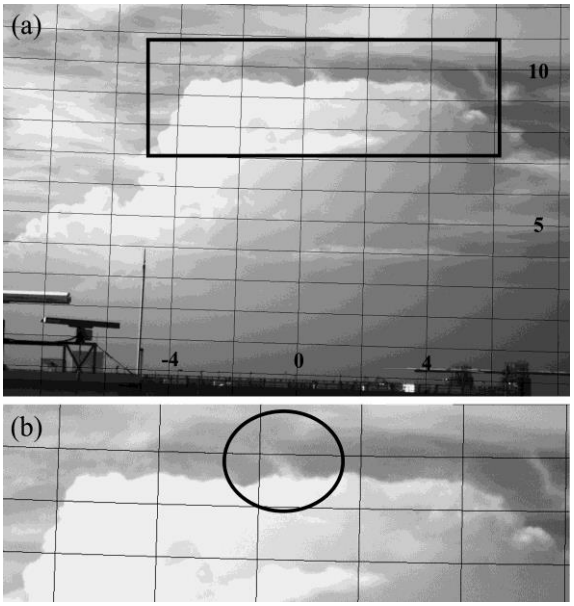

Fig. 2 An example of photographs of the JC taken from the NDA when the JC reached the highest altitude. It occurred at 15:39 in the Japan standard time (JST), Aug 10th, 2018 in Saitama. For better visibility, the sharpness, brightness, and contrast of the images have been adjusted. Horizontal and vertical lines denote the elevation and azimuth angles by 1° and 2° increment, respectively. (b) The bottom picture is a magnification of the area bounded in thick black in the upper one (a). The calculated altitude of anvil top is 15.3 km. The JC (denoted by the circle) jumped at the speed of 7.4 m s^{-1}, reached maximum height of 16.1 km, drifted westward, and dissipated in about 10 minutes (we could not exactly see the exact end because other clouds cut across the sight).

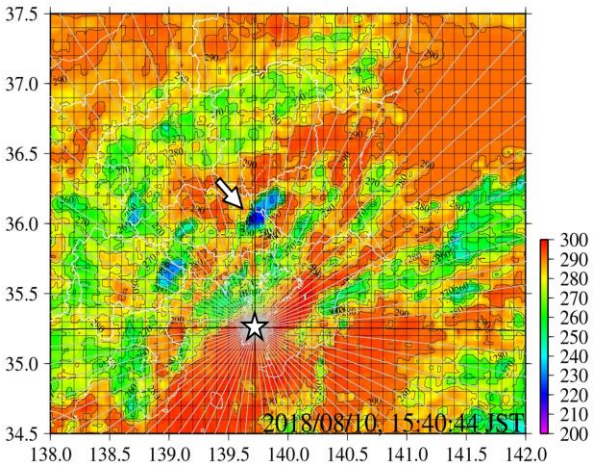

Fig. 3 The distribution of Infrared BT at 15:40 JST observed by the AHI band 13. The color shows BT [K]. The star symbol denotes the observation point, NDA. The radial gray lines from the observation point is azimuth angles by 5° increment. The arrow points the anvil of the cumulonimbus which lies in the azimuthal direction defined by the photograph. The coldest BT within the cloud top is 216.5 K at 36.04 °N, 139.68 °E, and 86.3 km from the NDA.

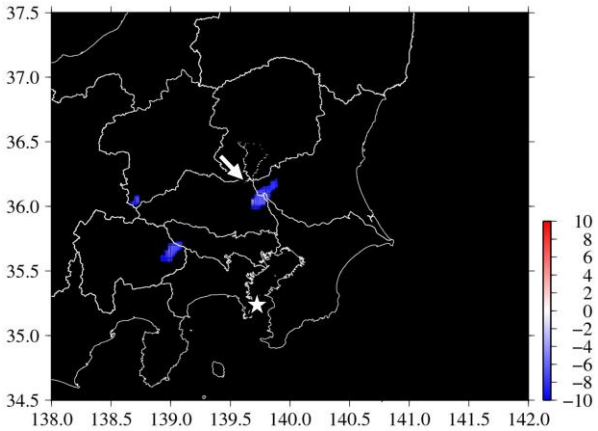

Fig. 4 The same as Fig. 3 but BTD [K]. Positive value means that the BT from band 8 is higher than band 13.

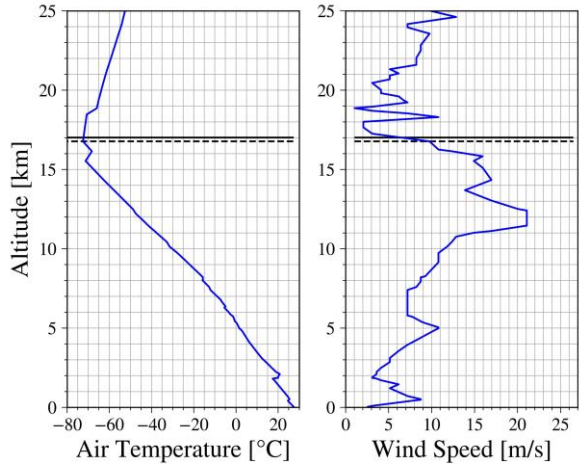

Fig. 5 The vertical profile of air temperature and wind speed at Tateno, 21:00 JST, 10th Aug 2018. The solid and dashed lines denote the lapse rate tropopause (LRT, 17.0 km) and the cold point tropopause (CPT, 16.8 km). The CAPE was 548.0 J kg^{-1} at that time. The wind shear between the altitudes of JC and anvil top was -3.2 m s^{-1} km^{-1}. The negative value means that the wind speed is smaller in the higher altitude.

2.4 *Ground-based Weather Radar*

To inspect the characteristics of the deep convections causing the JC as a precipitation system, we utilized two types of X-band radars.

One is the extended radar information network (XRAIN) operated by the Ministry of Land, Infrastructure, Transport and Tourism, Japan. The XRAIN consists of 39 multiparameter (MP) X-band radar sites all across Japan and mainly covers urban areas. The specification is: 9.7 GHz frequency, 150 m range resolution, and 1.2° azimuthal resolution. For our JC cases around Kanto, we can use the data from six sites.

Another is the phased array weather radar (PAWR). It has 9.4 GHz frequency and a better range resolution of 100 m. The number of the PAWR is six in Japan, and only the one at the Saitama site has a MP function. In our cases, one JC occurred in Saitama (Fig. 2) was measured by the MP-PAWR.

The most distinct feature of those is the temporal resolution of volume scan. Particularly, the PAWR takes a volume scan every 30 seconds with 100-step elevation angles, which is useful to continuously observe the vertical and internal structure of deep convective clouds that changes in the order of minutes, while the XRAIN does every 5 minutes with 20-step elevations. The maximum range is about 60 km for both radars.

3. RESULTS AND DISCUSSIONS

3.1 *Distribution of JC*

In our observation, many cases tended to be observed in the mountainside. This is reasonable for the cumulonimbus which forms when the air parcels are forced to rise by the terrain. Saito and Kimura (1998) statistically shows that a peak of the precipitation from deep convections lies in the afternoon in the Kanto region and the peak moves from the mountainside to the coastlines through 13-19 JST. Similarly, the 26 of total 28 cases occurred in the afternoon, and especially 20 cases occurred during 15-18 JST near the mountainside in our cases. These facts suggest that the occurrence of the JC and cumulonimbus have consistency, and thus JC is likely to be common for deep convective storms. There would be potentially more JC occurred but cameras could not observe them because the low-level cloud and local precipitation at the ground often interrupted the cameras' sight. Especially in August 2017, Kanto area experienced the 21 successive rainy days, which causes the less observed JC.

The possible explanations for less observed JC in the plain region are: (1) the cloud top of the large cumulonimbus occurred in the plain could not be seen because the plain area is relatively closer to the observation places. (2) as mentioned above, the peak of cumulonimbus formation is later at dusk in the plain area, hence, we could not see the JC.

3.2 *Characteristics of JC*

Seguchi et al. (2019) shows that their cases had smaller values of CAPE and environmental vertical wind shear above the anvil, while the height, vertical speed, and duration to disappear of the JC showed similar scales on average, compared with the case of JC in the US reproduced by three-dimensional non-hydrostatic cloud model simulations (Wang 2003, 2004 and Wang et al., 2011).

Now in this study, the new 14 cases have been added to the analyses (Table 1). Table. 1 shows the average value and standard deviation of several parameters for total 28 cases. However, the tendency described above did not change. It strengthens the inference that JC can occur even if the underlying convection is relatively weak and not a supercell thunderstorm like the US case. Also, Fig. 6 shows that the parameters of JC still have wide variations with each case. All correlations between the JC and

Table.1 The average and standard deviation (SD) of parameters of JC, the underlying anvil, and environmental atmospheric conditions for total 28 cases. For a comparison, the values resulted from numerical model simulations by Wang (2003, 2004) and Wang et al. (2011) are put down together if applicable. The number in the upper row is averages and SDs, and the one in the bottom is model results. The definition or how to calculate each value are discussed in the section 2.

	Jumping Cirrus				Anvil		Atmosphere	
	Jumping Height [km]	Width [km]	Vertical Jump Speed [m/s]	Duration [s]	Altitude [km]	Cloud Top Temperature [K]	CAPE [J/kg]	Wind Shear [m/s/km]
Average	1.3	2.3	9.3	747	13.7	223.7	727.1	-1.1
±SD	±0.5	±1.65	±5.4	±485	±1.9	±10.6	±544.9	±3.9
Model	1-3	5-15	8-10	360-	13	210	3312.5	1.6-12.5

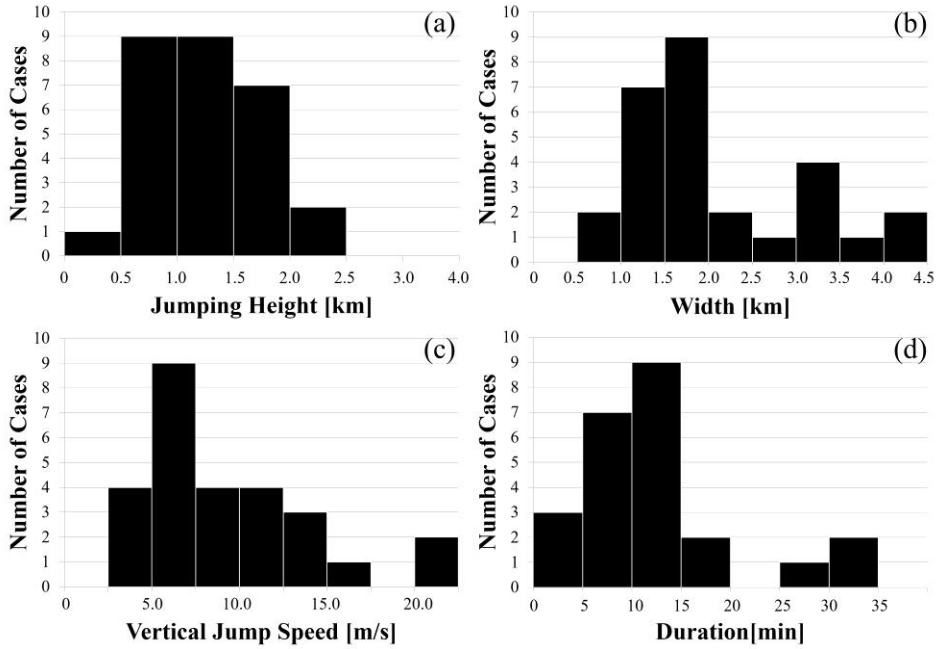

Fig. 6 Frequency distribution of JC parameters for all 28 case in 2016-18: (a) jumping height denotes the difference between altitudes of JC and anvil top, (b) width of a certain side of JC observed by cameras, (c) vertical jump speed denotes the average speed at which JC reached the highest altitude from the anvil top, and (d) duration denotes the time to disappear from the cameras' sight.

environmental parameters such as CAPE, anvil size, and environmental wind shear were weak (not shown). These results suggest that the JC parameters are not related to the magnitude of convection. However, we should be more cautious about the results. To understand the factors defining JC parameters, more observations and analyses are required. In particular, it is needed to compare the JC parameters with the OT ones such as the size of OT and time lag between OT and JC, since a JC is estimated to be caused by the breaking of gravity wave which a sinking OT creates. The OT parameters may indicate the local magnitude of the convection instead of CAPE. As for the calculation of wind shear above the anvil, the storm-relative wind may be more appropriate rather than the environmental wind. These because the sounding data from radiosonde such as CAPE and environmental wind may not represent the exact value to express the state of the local convections.

3.3 *Possibility of the Hydration of LS*

The six cases of JC entered the LS based on the atmospheric soundings at Tateno. However, the other cases possibly entered the LS, too because the existence of the anvil itself may indicate the tropopause or inversion layer. As for the case of Fig. 2, the top of JC was lower than the tropopause. Also, the temperature profile shows that there was an inversion layer near the anvil top altitude (at 15.3 km, Fig. 5). Thus, this case shows that the JC occurred from the anvil made at inversion layers.

On the other hand, water vapor amount in the LS was not enough to be detected by use of BTD method for all cases. In the case of Fig. 2, the BTD value shows negative (Fig. 4). When the JC was under the tropopause, it is natural because air temperature is lower in higher altitude within the troposphere where the above anvil is. It is worth noting that even if the JC reached the tropopause, the BTD does not always become positive. For instance, it may happen when the temperature gradient is too small where there is the layer of neutral buoyancy in the LS or when the LS water vapor amount is too small to be detected by satellites.

3.4 *Properties of Precipitation Cells under the JC*

Fig. 7 illustrates a structure of precipitation recorded by the MP-PAWR when the JC in Fig. 2 reached the highest altitude. For a comparison, Fig. 7a is adjusted to the view from the camera (Fig. 2). Because we cannot locate the exact point of the JC, the cross section along the strongest convection is shown in Fig. 7. The motion of rapid vertical development of the precipitation cell (along about 139.67 °E in Fig. 7a, not shown) are well accorded with the apparent growth of the cloud by the camera observations. The echo top height of about 15 km is also consistent with the anvil top of 15.3 km in Fig. 2. However, the jumping cirrus was not recorded by the MP-PAWR. The Cloud Profiling Radar on the polar orbiting satellite CloudSat, whose wavelength is 94 GHz (W-band), could detect the JC as about -20 dBZ (Wang et al., 2011). It implies that the JC is composed of tiny ice particles. It is usually difficult to visualize the small cloud particles with X-band radar. However, if JC has the same size particles as its underlying anvil, it is possible for the JC to be detected by X-band. Some research report that the anvil cloud of severe supercell was visualized as about 16 dBZ (Kobayashi et al., 2001). In Fig. 7, the MP-PAWR shows the minimum sensitivity for about 10 dBZ at about 20 km distant place from the radar site. Currently, the available ground radar network is only C and X-band radars. Thus, if we can utilize them to see the JC and anvils, it is helpful for the study of cloud top phenomena.

Seguchi et al. (2019) utilized C-band radar (5.3 GHz) data operated by Japan Meteorological Agency to investigate the relation between the storm severity and JC. They found that the 14 cases of thunderstorms causing JC were accompanied with heavy rain which was more than 100 mm h^{-1}. They also examined the time variation of the maximum estimated precipitation intensity at the ground originated from the precipitation cell under the JC (like Fig. 8), but no distinct changes were found before and after the JC occurred. This would be because C-band radar data has inadequate interval which is only every 10 minutes. For the same kind of investigations, the XRAIN and the PAWR is useful with their higher observation frequency (60 and 30 seconds, respectively).

Fig. 7b shows the estimated rain rate at the ground by the MP-PAWR. In this case, the northwest, the northeast, and the southeast from the radar site partly lack the data due to the interruption by obstacles and wave attenuation by heavy rain. However, we can recognize the heavy rain of about 60 mm h^{-1} from the cell under the JC.

Fig. 8 shows the time series of the maximum value of rain rate within the precipitation cell under the JC of Fig. 2 for an hour before and after the JC occurred. In this case, many cumulonimbus clouds occurred around the time. Especially, the cell which generated the JC appeared to be a part of the multicell cloud system. The cell generating the JC itself started to develop rapidly around 15:25. The growth speed was estimated to be about 12.9 m s^{-1} by the camera observation. At around 15:31, the cloud reached the level of neutral buoyancy, made anvil, and the OT stated to rise upward. During the span, the radar reflectivity of the precipitation core

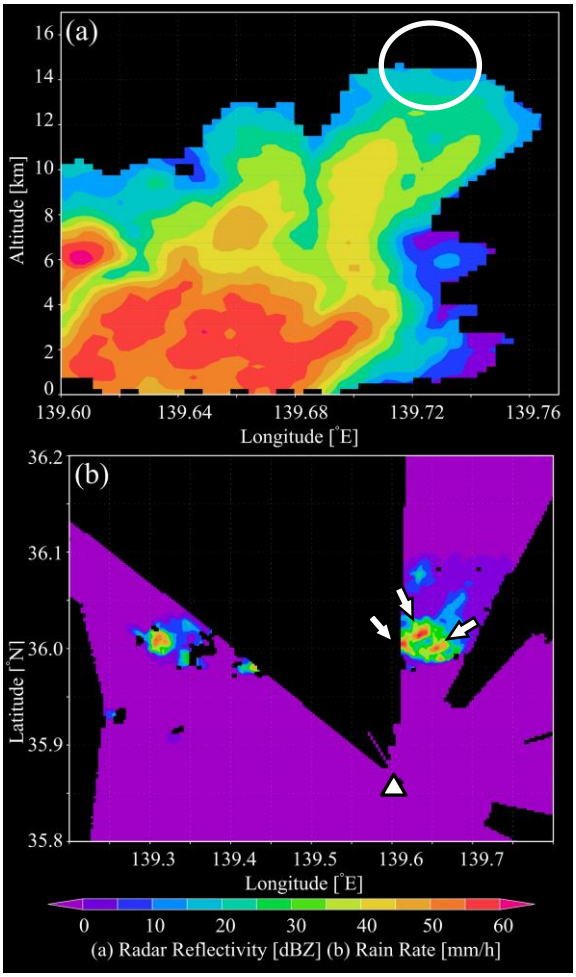

Fig.7 (a) the radar reflectivity of altitude-longitude cross section along 36 °N and (b) estimated rain rate at the ground (250 m). Both were recorded at 15:39:30 when the JC reached the highest altitude of 16.1 km. The color bar scale is common for both parameters. The area surrounded by the white circle corresponds to the black circle in the Fig. 2. The triangle symbol denotes the MP-PAWR radar site (Saitama, 35.86 °N, 139.61 °E). The three arrows indicate the three different precipitation cells of the multicell storm.

showed the maximum of 60 dBZ at around 2-6 km height (not shown) and the rain rate at the ground increased to the maximum over 200 mm h^{-1}. Then, during the anvil making, the radar reflectivity of the core and the ground rain rate gradually declined. After that, the OT reached the highest altitude at 15:33 and sank at 15:39 in about 6 minutes. Mostly at the same time, the JC occurred at 15:39, which means the lead time of the JC from the OT was about zero. The distance between where the JC and the OT rose were about 2 km though it is not known whether the lead time and the distance are related. During 15:31-15:39, the ground rain rate had a peak at around 15:35 but it is slightly different from the peak of the OT height at 15:33. When the JC occurred, the cloud started decaying as the radar reflectivity of the core and the ground rain rate decreased. Totally, the time variation of the parameters shows a complicated behavior. This is partly because the maximum value of the rain rate included the

different cells of the multicell storm, which may be three red areas shown in Fig. 7b. Further examinations for other cases are required to find the statistical relation between the JC and the precipitation.

For further work, we need more additional investigations using the data from X-band radars. For example, in order to explore the characteristics of JC, it is helpful to scrutinize the cause of cumulonimbus formation for each JC case. This can be achieved by examining the wind field (doppler velocity) at the ground and above anvil, vertical wind shear, and motion of deep convective storms seen from the AHI visible bands. To explore the statistical relation between the JC and the precipitation, comparisons between deep convective storms which caused JC and which did not are required. However, the statistical data of the precipitation in previous studies cannot be utilized because they did not take into account the JC. Therefore, we need to newly prepare the cases of deep convections which did not create the JC for a comparison.

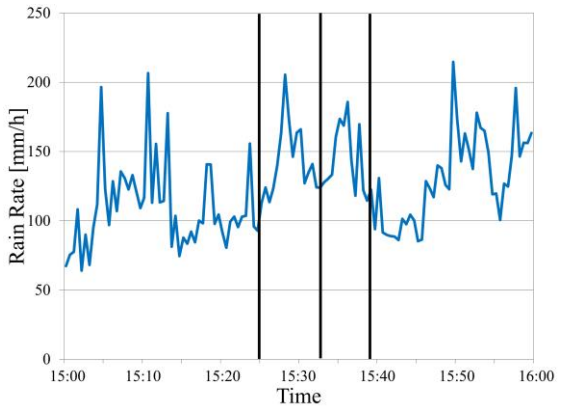

Fig. 8 The time series of the maximum value of rain rate within the precipitation cells under the JC recorded by the MP-PAWR in Saitama. From the left, the three vertical lines denote the time when (1) the cumulonimbus rapidly developed at 15:25 JST, (2) the OT reached the highest altitude at 15:33 JST, and (3) the OT sank and the JC jumped at 15:39 JST.

4. SUMMARY AND CONCLUSION

In this study, we analyzed the characteristics of the JC and the underlying deep convective storms together with the environmental atmospheric conditions and precipitation systems. We found totally 28 cases of the JC during the summer in 2016-18, around the Kanto region, Japan. The analyses of the JC and atmospheric parameters revealed that the JC occurred even from evidently weaker convections which sometimes did not reach the tropopause. Consequently, the sounding by a radiosonde showed that the number of cases where the JC entered the LS was six. The BTD method could not detect the water vapor layer in the LS in our cases.

This is the first study to show the relation between the JC and the precipitation system using the MP-PAWR. It is still difficult to record the JC by X-band radars due to their sensitivity, but it shows the potential to investigate the statistical analyses of the relation between the JC and precipitation with their high frequent observation.

The point is that the JC is likely to be a common phenomenon while its observation is difficult. To understand more about the JC, we need various physical properties from many instruments and more cases at various places. It may be difficult to record the JC by the current ground radar network, but it is not impossible by using other algorithms to process the raw data and other wavelength measurements. Also, we would like to emphasize that the camera observation is one of the most effective method to record the many case of the JC at present.

ACKNOWLEDGEMENTS

This work was supported in part by the Collaborative Research Program of Research Institute for Applied Mechanics, Kyushu University, and JSPS Kakenhi JP17H06139 and JP19K12314. The observation at Mt. Fuji was performed at the Mt. Fuji Weather Station, which is currently managed by the Mount Fuji Research Station (MFRS), a nonprofit organization certified by the government of Japan. They helped to support our work, including the installation and maintenance of the cameras. The data from Himawari-8 were obtained from the NICT Science Cloud at National Institute of Information and Communications Technology. The radiosonde data were obtained from the Department of Atmospheric Science, University of Wyoming. MP-PAWR was developed as a part of the Strategic Innovation Promotion Program by the Cabinet Office of Japan and the data were offered by the National Research Institute for Earth Science and Disaster Resilience.

REFERENCES

Fujita, T. T., 1974: Overshooting thunderheads observed from ATS and Learjet. *Satellite and Mesometeorology Research Project Rep.* 117, 29 pp.

Fujita, T. T., 1982: Principle of stereoscopic height computations and their applications to stratospheric cirrus over severe thunderstorms. *J. Meteor. Soc. Jpn.*, 60, 355–368.

Homeyer, C. R., J. D. McAuliffe, and K. M. Bedka, 2017: On the development of above-anvil cirrus plume in extratropical convection. *J. Atmos. Sci.*, 74, 1617–1633.

Kobayashi, F., Y. Ueno, N. Inatomi, and T. Shimura, 2001: The cumulonimbus causing heavy rain around the urban area in Tokyo on July 21st 1999, *Tenki*, 48, 3-4. (in Japanese)

Saito, T., and F. Kimura, 1998: Diurnal variation of convective precipitation in Chubu-Kanto area in the summer. *Tenki*, 45, 541-549. (in Japanese)

Seguchi, T., S. Iwasaki, M. Kamogawa, T. Ushiyama, and H. Okamoto, 2019: Observation of jumping cirrus with ground-based cameras, radiosonde, and Himawari-8. *J. Meteor. Soc. Jpn.*, 97, 615–632.

Setvák, M., D. T. Lindsey, R. M. Rabin, P. K. Wang, and A. Demeterová, 2008: Indication of water vapor transport into the lower stratosphere above

midlatitude convective storms: Meteosat Second Generation satellite observations and radiative transfer model simulations. *Atmos. Res.*, 89, 170–180.

Setvák, M., K. Bedka, D. T. Lindsey, A. Sokol, Z. Charvát, J. Šťástka, and P. K. Wang, 2013: A-Train observations of deep convective storm tops. *Atmos. Res.*, 123, 229-248.

Wang, P. K., 2003: Moisture plumes above thunderstorm anvils and their contributions to cross-tropopause transport of water vapor in midlatitudes. *J. Geophys. Res.*, 108, 4194.

Wang, P. K., 2004: A cloud model interpretation of jumping cirrus above storm top. *Geophys. Res. Lett.*, 31, L18106.

Wang, P. K., M. Setvák, W. Lyons, W. Schmid, and H.-M. Lin, 2009: Further evidences of deep convective vertical transport of water vapor through the tropopause. *Atmos. Res.*, 94, 400–408.

Wang, P. K., S. H. Su, Z. Charvát, J. Šťástka, and H.-M. Lin, 2011: Cross tropopause transport of water by mid-latitude deep convective storms: A review. *Terr. Atmos. Ocean. Sci.*, 22, 447–462.